*Ceramics International* **23** (1997) 489–496

PII: S0272-8842(96)00059-4
0272-8842/97 $17.00+.00

# Effect of Coal Slag on the Wear Rate and Microstructure of the $ZrO_2$-Bearing Chromia Refractories

**Zong-Qi Guo,[a] Bo-Qi Han[b] & Hai Dong[c]**

[a]Luoyang Institute of Refractories Research, 43 Xiyuan Road, Luoyang, Henan 471039, P. R. China
[b]Lunan Fertilizer Plant, Tengzhou, Shandong 277527, P. R. China
[c]Xinxiang Refractory Factory, Xinxiang, Henan 453000, P. R. China

(Received 24 January 1996; accepted 2 May 1996)

**Abstract:** The typical properties of slag and refractories for slagging coal gasifier were investigated. In the range of 0–25% CaO/ash, the characteristic ash-fusion temperatures (AFTs) and viscosity of a coal-ash slag decreased with an increase of CaO additive. When the CaO/ash ratio was greater than 25% in the mixture of the coal and limestone, AFTs no longer reduced. The slag viscosity for limestone addition with CaO/ash = 25% was very low and in a narrow range (4–13 Pa·s) at coal gasification temperatures between 1300°C and 1500°C. However, corrosion resistance of the $ZrO_2$-bearing chromia refractories reduced with increasing CaO content in coal slag, especially for a slag with more than 30% CaO content. Increased chromia in three kinds of the $ZrO_2$-bearing chromia refractories resulted in increased corrosion resistance. The higher the $Cr_2O_3$ content and the lower the $SiO_2$ content, the less the deterioration of microstructures in the materials. Thermochemical spalling of the $ZrO_2$-bearing 80% $Cr_2O_3$ refractory after 807 operating hours of a coal gasifier was considered as the primary attack mechanism. © 1997 Elsevier Science Limited and Techna S.r.l.

## 1 INTRODUCTION

The maximum solubility of $Cr_2O_3$ in coal slag is very low at high temperature.[1] The gasifiers operated at high temperature and high pressure are all lined with high chrome refractories, among which $Cr_2O_3$–$Al_2O_3$–$ZrO_2$ refractories are prime candidates.[2]

In the Texaco coal gasification process, the gasifier temperature must be high enough to assure continuous flow of slag from the gasifier, but yet not so high that it may lead to other operating and maintenance problems, such as excessive refractory wear or decreased burner life. Corrosion–erosion phenomena of the gasifier's brick lining cannot be totally eliminated at 1400–1600°C, but an understanding of the high temperature fusion behaviour of coal-ash slag and the chemical interaction between slag and refractories enables the corrosion–erosion rate of refractories to be reduced to a minimum, i.e. the service life of a gasifier's refractory lining can be prolonged by good control of the process conditions.

Therefore, the high temperature behaviour of coal slag is very important for the coal gasification process and refractory life. The present paper reports on a study of the effect of coal ash composition on ash-fusion temperatures, slag viscosity and the wear rate of $Cr_2O_3$–$Al_2O_3$–$ZrO_2$ refractories. The microstructural analysis was also conducted by optical microscopy and scanning electron microscopy.

## 2 EXPERIMENTAL

The chemical compositions of Qiwu coal ash and limestone (used as a fluxing agent in the present study) are given in Table 1.

The ground Qiwu coal was mixed with the fine limestone in designed proportions. The mixture was fired at 815°C, then cooled and ground so as to

**Table 1. Chemical analysis of Qiwu coal-ash and limestone (wt%)**

| Oxide | $SiO_2$ | $Al_2O_3$ | $Fe_2O_3$ | CaO | MgO | $TiO_2$ | $K_2O$ | $Na_2O$ | $SO_3$ | $CO_2$ |
|---|---|---|---|---|---|---|---|---|---|---|
| Coal-ash | 48.91 | 30.61 | 4.20 | 7.82 | 2.67 | 0.91 | 0.35 | 0.18 | 2.45 | — |
| Limestone | 1.65 | 0.32 | 0.67 | 52.34 | 2.31 | — | — | — | — | 40.28 |

obtain an even, fine coal-ash specimen. Addition of fluxing agent is determined by the percentage of efficacious addition of CaO/coal-ash. The coal-ash fusion test, performed according to the national standard GB219-74, consisted of observing triangular pyramids of coal-ash–additive mixtures in a furnace in which the temperature was continuously increasing. The characteristic ash-fusion temperatures (AFTs) included deformation temperature (DT), softening temperature (ST) and fluid temperature (FT). Viscosity was determined by a ND-3 high-temperature-rotary digital viscometer. The refractory samples included new bricks obtained directly from their manufacturer and a section of a used brick removed from a Texaco gasifier. The routine properties of the new bricks were determined. Laboratory tests for corrosion resistance were conducted in a graphite crucible, into which the coal-ash was introduced. 20×20×150 mm test bars were rotated in the slag at 1600°C for 4 h. Small cores taken from the as-manufactured brick and the used brick were polished and examined by optical microscopy with the help of scanning electron microscopy and X-ray diffraction.

## 3 RESULTS AND DISCUSSION

### *3.1 Ash-fusion temperatures and viscosity of coal-ash slag*

The characteristic ash-fusion temperatures, DT = 1330°C, ST = 1350°C and FT = 1460°C, are too high for Qiwu coal to be gasified. It is necessary to add limestone as a fluxing agent. AFTs basically decrease with an increase of CaO additive, except for the highest ST with 5% CaO/ash additive. When the CaO/ash ratio is greater than 25% in the mixture of Qiwu coal and limestone, it seems that AFTs no longer reduce. The change of AFTs with an increase of CaO additive is shown in Fig. 1.

Huggins' study[3] indicated that the two most important chemical parameters determining AFTs were percent base and $SiO_2/Al_2O_3$ ratio for coal-ash compositions in which $Al_2O_3 + SiO_2$ exceeds 70%. Except for a little displacement in percent CaO, the experimental AFT curves would closely parallel the liquidus with CaO across the CaO–$SiO_2$–$Al_2O_3$ equilibrium diagram along the line of $SiO_2/Al_2O_3$ in coal-ash. The displacement can be attributed to the presence of other basic oxides. Figure 1 further confirmed that the $Al_2O_3$–$SiO_2$–base phase diagram could provide some information for determining what additive and what dosage are needed to gasify coal with high ash-fusion temperatures.

Viscosity–temperature curves for coal slags are shown in Fig. 2. The viscosity of coal slag is significantly reduced by CaO addition. At temperatures between 1300°C and 1500°C, which is the usual operating temperature range of a Texaco coal gasifier, viscosity fluctuation of coal slag with 25% CaO additive is very narrow (4–13 Pa·s). This permits the slag to tap smoothly. Even though the temperature in the gasifier is as low as 1250°C, it was proved that slag with a viscosity of 23 Pa·s had enough fluidity to prevent tap hole plugguge in a pilot plant.

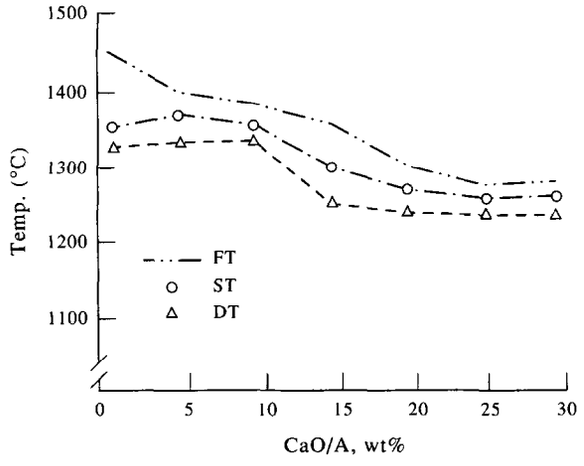


**Fig. 1.** Change of AFTs with CaO addition in Qiwu coal-ash.

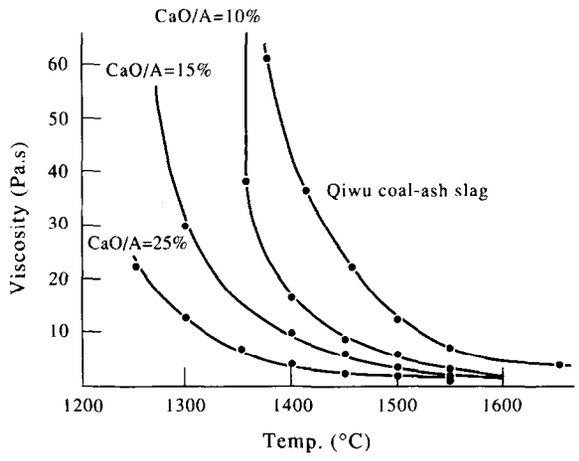


**Fig. 2.** Viscosity–temperature curves for coal slags.

Slag is a non-ideal solution made up of complex anions formed by the reaction of "acidic" cations with oxygen ions generated by the dissociation of the "basic" oxides. The typical acidic component, silicon, reacts with oxygen ions to form complex anions:

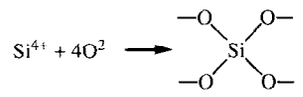

and if there are not enough free oxygen ions to satisfy the complexation requirements, these anions will share oxygens by polymerization.

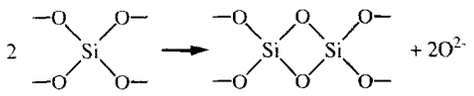

But bases donate oxygen ions to the solution by the disassociation reaction, such as

$$CaO \rightarrow Ca^{2+}O^{2-}$$

It is the balance of these acid–base components and their interaction that determine the viscosity of the slag. Let's assume initially that quartz is the only mineral in coal. Quartz could melt and be converted to a highly polymerized slag. This slag would be expected to be very viscous. However, if basic components, such as lime, are also present with quartz, they would donate oxygen ions which would break down many of the polymeric bonds in the slag structure and a less viscous slag would be anticipated. The schematic in Fig. 3 is a simplified simulation of how the acid/base components transform and interact to determine the final slag viscosity.

### 3.2 Properties of $Cr_2O_3$–$Al_2O_3$–$ZrO_2$ refractories

The test results of $Cr_2O_3$–$Al_2O_3$–$ZrO_2$ bricks are listed in Table 2. Obviously, compared to Brick-S and Brick-E, the $SiO_2$ content reduces and the $Cr_2O_3$ content increases in Brick-N. This leads to improvement of the hot modulus of rupture. The thermal shock resistance of Brick-N is much better than those of Brick-S and Brick-E. Corrosion resistance of the bricks exposed to coal slags with various CaO content is shown in Fig. 4. $Cr_2O_3$ content is important to reduce corrosion rate, no matter what type of slag the bricks are exposed to. The decline is considered to be related to the loss of soluble components in the composition as the materials are stabilized by the increasing amount of chromia.

In Fig. 4, the corrosion rate of the test materials increases with an increase of CaO content in the coal slag. The three curves all show a steep increase in corrosion rate when the CaO content in the slag surpasses 30%. They also have almost the same tendency, which is a strong indication that a change in the properties of the molten slag has a direct bearing on the corrosion rate in the present test.

The corrosion rate is a phenomenon which is strongly dependent on viscosity, solubility, temperature and amount of slag per unit of time. So for given bricks and process conditions in the present test, the corrosion rate was most dependent on the slag viscosity. A slag with lower viscosity easily penetrates into refractory pores, leading to more corrosion. The change of the corrosion rate in

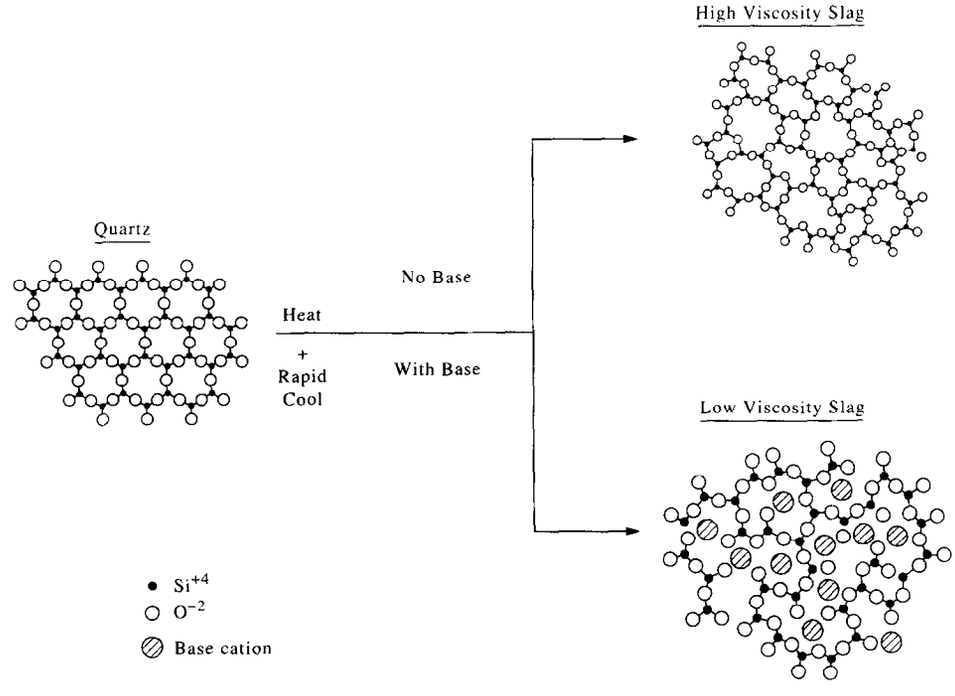


**Fig. 3.** Principle scheme showing slag viscosity being lowered by base addition.

Fig. 4 is mainly attributed to the viscosity decline with the increase of CaO content in the slag, as shown in Fig. 2.

**Table 2. The properties of $Cr_2O_3$–$Al_2O_3$–$ZrO_2$ bricks**

| Property | Brick-S | Brick-E | Brick-N |
|---|---|---|---|
| Chemical analysis (wt%) | | | |
| $SiO_2$ | 6.28 | 3.21 | 0.60 |
| $Al_2O_3$ | 16.24 | 8.26 | 3.46 |
| $Fe_2O_3$ | 0.22 | 0.22 | 0.15 |
| $TiO_2$ | 0.79 | 1.22 | 1.38 |
| $ZrO_2$ | 11.48 | 4.42 | 6.02 |
| $Cr_2O_3$ | 61.78 | 80.56 | 87.29 |
| Apparent porosity (%) | 9 | 13 | 15 |
| Bulk density (g/cm$^3$) | 3.90 | 3.95 | 4.23 |
| Cold crushing strength (MPa) | 202.4 | 123.2 | 118.2 |
| Modulus of rupture at 1400°C (MPa) | 9.88 | 9.86 | 13.2 |
| Thermal shock resistance (1100°C–water cooling) (cycles) | 2 | 1 | 16 |
| Creep ratio under 0.2 MPa (1500°C, 30 h) (%) | 0.586 | 0.417 | 0.837 |

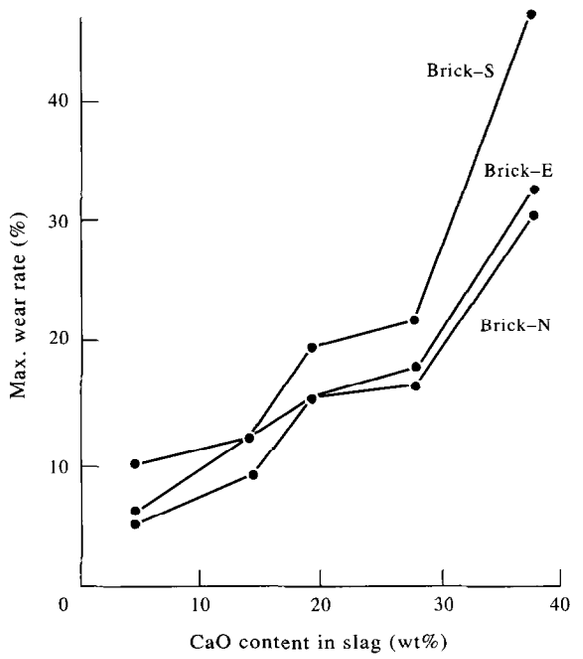


**Fig. 4.** Corrosion rate of the test bricks exposed to coal slag with various CaO content.

### 3.3 Microstructural analysis

#### 3.3.1 The freshly-manufactured bricks

Brick-S: There are two kinds of grains in the microstructures of Brick-S. One is found in the eutectoid structure, with 60–120 $\mu$m×12–90 $\mu$m tabular $(Cr, Al)_2O_3$ crystals containing 20% round granular baddeleyite of 12–90 $\mu$m diameter, which appears to be green in the cores (reflectivity of 12.3%) and rose colour at the periphery (reflectivity of 9.3%), indicating a higher $Cr_2O_3$ content in the centre than at the fringe. Another kind of grain consists of green $Cr_2O_3$ crystals (reflectivity of 16.4%), in which there are some pores of 2–6 $\mu$m diameter, as shown in Fig. 5(a). The matrix of Brick-S consists of granular $(Cr, Al)_2O_3$ with a great disparity in crystal dimensions (large ones up to 36–48 $\mu$m and small ones down to 6–12 $\mu$m) and deformed worm-shaped $(Cr, Al)_2O_3$ crystals (10–15 $\mu$m) around monoclinic zirconia (~30 $\mu$m in diameter) with microcracks. $ZrO_2$ grains are agglomerated, as shown in Fig. 5(b). The crystals mentioned above are joined by a glassy phase that shows basal plane and accounts for 30% of the matrix.

Brick-E: There are $Cr_2O_3$ aggregate particles, 1160–1624 $\mu$m in dimension, bonded by a matrix of $(Cr, Al)_2O_3$ solid solution and $ZrO_2$. The photo micrograph in Fig. 6 shows that grains in the brick are primarily composed of 25–54 $\mu$m diameter chromium oxide crystals, most of which are directly bonded and some of which have pores filled with glassy phase (~5%). The matrix of Brick-E is uneven and roughly classified into two regions: a $ZrO_2$-rich region and a $ZrO_2$-poor region. The $ZrO_2$-rich region consists of ~15% (21–45 $\mu$m diameter) zirconia crystals and 47–78 $\mu$m diameter deformed worm-shaped chromium oxide crystals (reflectivity of 16.6%). Approximately 25% glassy phase fills in between the crystals.

There is a large amount of porosity, up to 40%. The $ZrO_2$-poor region contains only 5% (10–

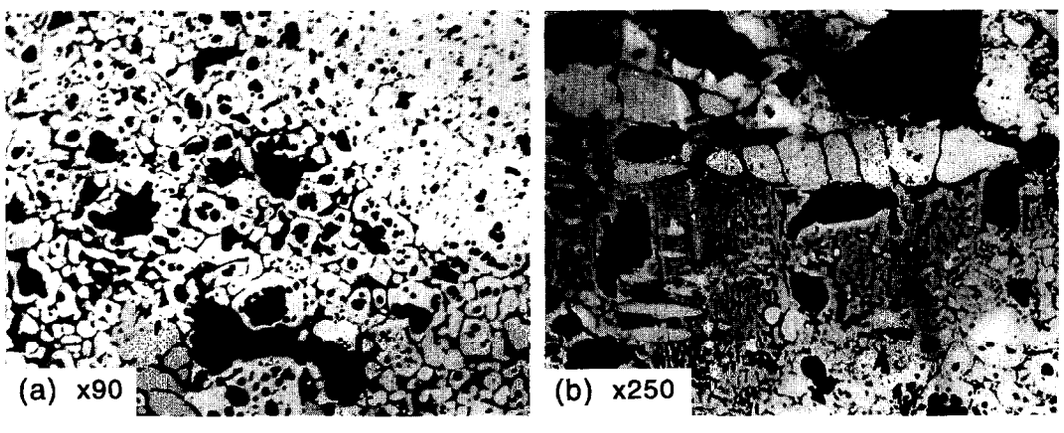


**Fig. 5.** Microstructures of Brick-S.

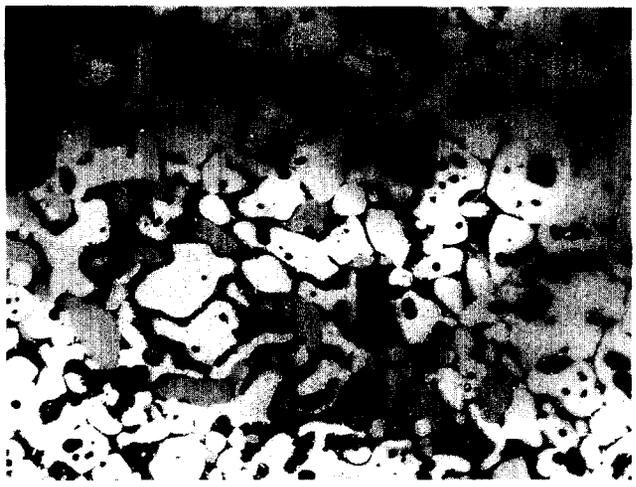

**Fig. 6.** Microstructure of Brick-E (×250).

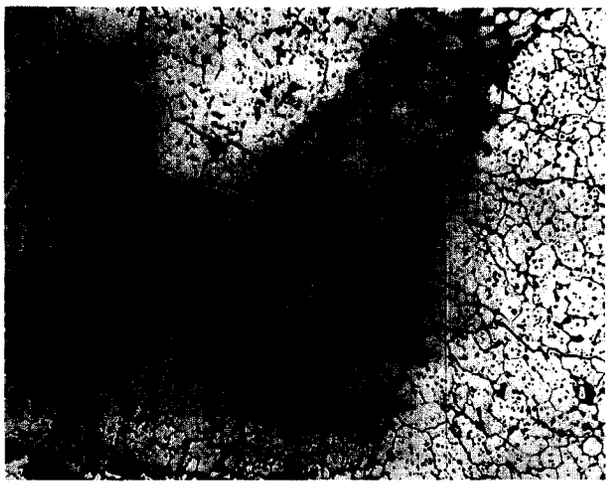

**Fig. 8.** Microstructure of Brick-N (×90).

18 $\mu$m diameter) granular $Cr_2O_3$ crystals that have 10–30 $\mu$m openings. Porosity occupies 15–20% of this region.

The second electron image (SEI) of Brick-E also indicates that 12–35 $\mu$m granular $Cr_2O_3$ as main crystals are interlaced by a small amount of $ZrO_2$ crystals, as shown in Fig. 7(a). Figure 7(b) shows that unevenly distributed zirconia crystals have been agglomerated and become pupa-shaped. Actually, there is a little $Al_2O_3$ dissolved in the $Cr_2O_3$ crystals. EDAX result for the matrix of Brick-E is $Al_2O_3$ 11.95%, $SiO_2$ 6.58%, $ZrO_2$ 10.88%, CaO 0.63%, $TiO_2$ 1.32% and $Cr_2O_3$ 68.63%, showing that most of the $Al_2O_3$ and $ZrO_2$ are present in the matrix.

Brick-N: The grains consisting of $Cr_2O_3$ in Brick-N show allotriomorphic granular crystals (16–75 $\mu$m diameter) with pores (1–7 $\mu$m diameter) and reflectivity of 16.4%. The main crystals of the matrix are 16–64 $\mu$m $Cr_2O_3$ crystals (reflectivity of 16.3%), which have 2–32 $\mu$m pores. 5–10% intergranular zirconia as minor crystals is situated in the interval of $Cr_2O_3$ crystals. There are 40% pores and 5–10% glassy phase in the matrix. Figure 8 shows the microstructure of Brick-N.

*3.3.2 Microstructural change after slag penetration*

After slag tests, three samples were examined, which were exposed to the same slag. The slag composition is as follows (wt%): $SiO_2$ 48.69, $Al_2O_3$ 22.92, CaO 17.88, $Fe_2O_3$ 2.88, MgO 1.43, $K_2O$ 1.15, $Na_2O$ 0.87 and LOI 1.7. Microstructural analyses demonstrate that microstructures of the slagged area for the three kinds of bricks tend to be stablized with increasing $Cr_2O_3$ content in the refractories. In Brick-S, chrome corundum containing $ZrO_2$ is dissolved by the molten slag, which fills in pores between crystals and cavities. The microstructure starts to change at a distance of 1160 $\mu$m from the working face. The region shown in Fig. 9(a) is full of anorthite and glassy phase. Recrystallized zirconia appears like a string of beads in the region 928 $\mu$m away from the working face, as shown in Fig. 9(b).

Slag penetration into Brick-E resulted in an increase of glassy phase and porosity, and the appearance of a network of $Cr_2O_3$ cracks, as shown in Fig. 10.

Due to slag penetration, $Cr_2O_3$ crystals in Brick-N rearranged and its microstructure densified. Granular $ZrO_2$ crystals still co-exist with the glassy

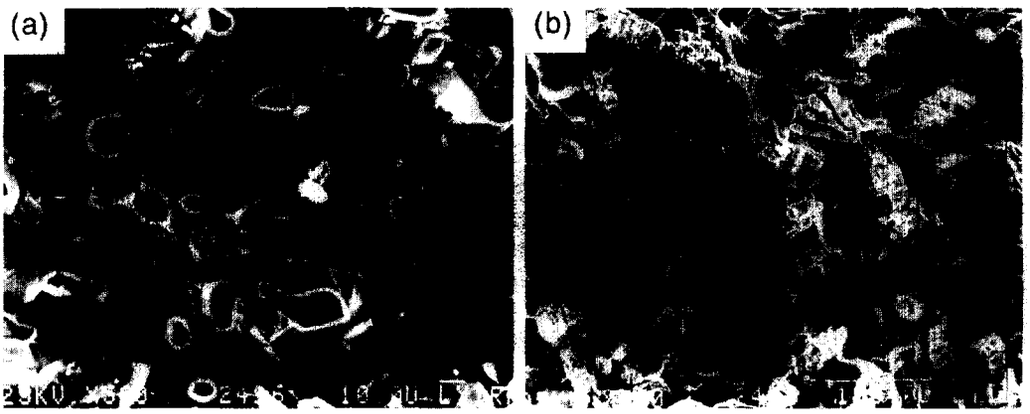


**Fig. 7.** SEI of Brick-E.

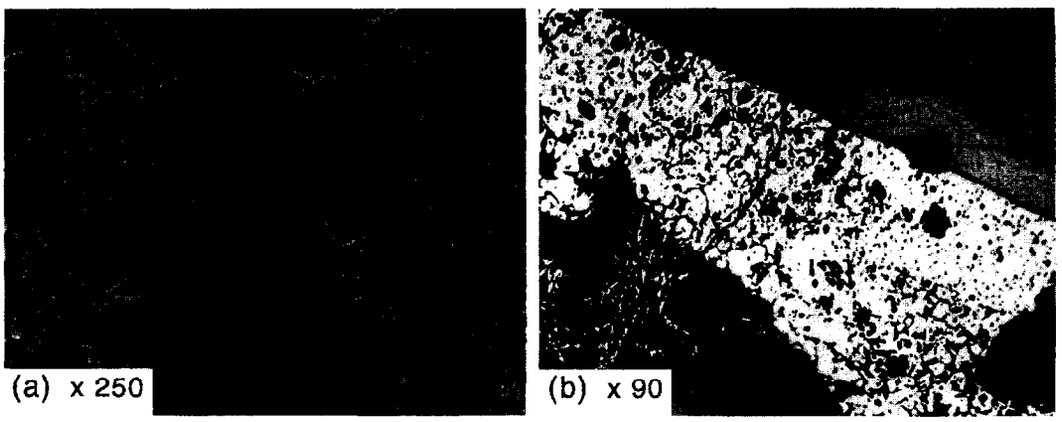


**Fig. 9.** The slagged region of Brick-S.

phase, as shown in Fig. 11. There is little change from the original microstructure. A comparison of the microstructural changes for the three types of bricks clearly demonstrates that the effect of slag penetration on microstructure is least for Brick-N, which has the lowest $SiO_2$ content and the highest $Cr_2O_3$ content.

*3.3.3 Microstructure of the used brick*

Only used Brick-E was examined in the present investigation. It had been cycled from ambient temperature to 1350–1700°C at least 20 times in a Texaco gasifier and had serviced for at least 807 h under coal residues before being removed for testing. The gasifier was fed on a mixture of Qiwu coal and limestone according to CaO/ash = 25% that was determined by above-mentioned viscosity–temperature curves.

The microstructural analysis on the used brick showed five zones, i.e. unaltered zone, transition zone, reaction zone, working zone and slag coated zone.

Transition zone (19.8–23.3 mm away from the working face): It retains the basic features of the unaltered zone or original brick. There is 20% crystalline zirconia in the matrix, most of which is 20–200 $\mu$m diameter tetragonal $ZrO_2$ showing spindle shape and irregular shape. It is noted that tetragonal $ZrO_2$ emerges in this zone and doesn't present in the others. A monoclinic $ZrO_2$ rim, with a width of 3–18 $\mu$m forms around the 2–5 $\mu$m tetragonal $ZrO_2$ granular crystallines.

Reaction zone (6.5–17.5 mm away from the working face): A glassy phase is increasingly evident in the reaction zone. Granular $Cr_2O_3$ crystals are joined by a glassy phase, which shows basal plane and accounts for 40% of the matrix. There is 10% gehenite ($2CaO{\cdot}Al_2O_3{\cdot}SiO_2$) in the matrix.

Working zone (5.8–6.6 mm in width): Coal slag entered the bulk of the zone by way of cracks. The brick began dissolving. Grains with a size of 1980 $\mu$m were found in the slag.

Figure 12 shows the microstructure of the used Brick-E. Upon contact with molten slag, $Cr_2O_3$ grains are enriched mainly with $Al^{3+}$ and $Fe^{2+}$ and/or $Fe^{3+}$ from the slag. $Cr_2O_3$–sesquioxide solid solution and complex spinel solid solution are formed around the grains. Part of the $Cr_2O_3$ dissolves slowly into the slag.

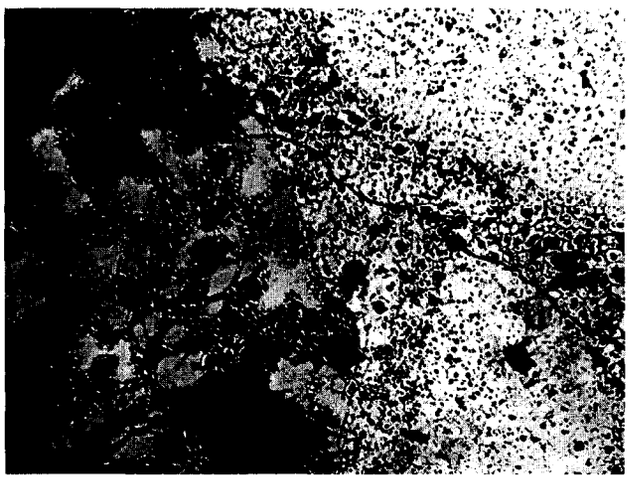

**Fig. 10.** The slagged region of Brick-E (×90).

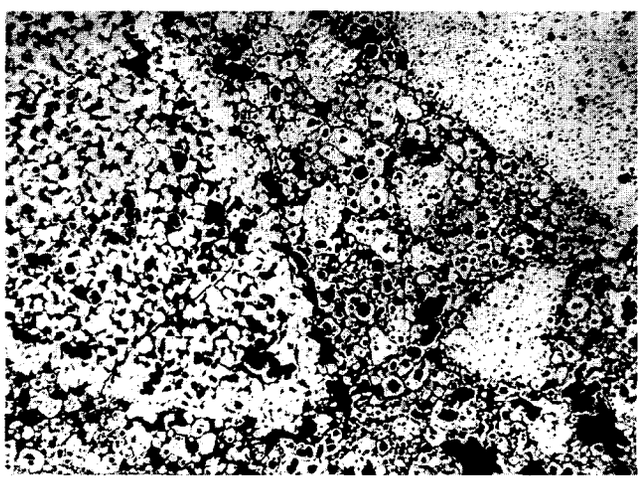

**Fig. 11.** Microstructure of Brick-N exposed to slag (×90).

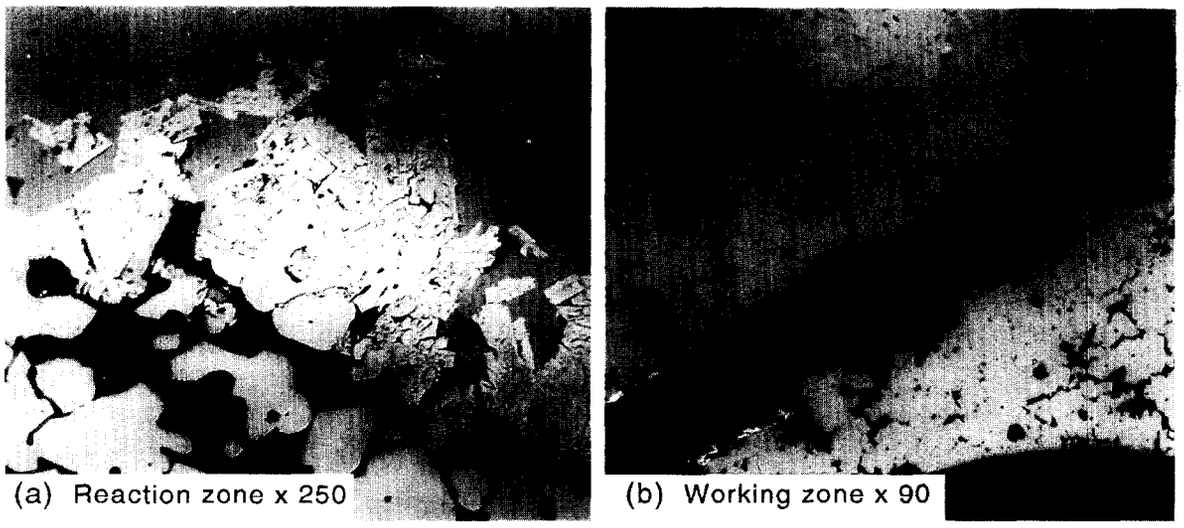


**Fig. 12.** Microstructure of the used Brick-E.

Table 3 lists the mineral composition of the slag upon contact with Brick-E in the gasifier. It is evident that gehlenite ($2CaO{\cdot}Al_2O_3{\cdot}SiO_2$) and anorthite ($CaO{\cdot}Al_2O_3{\cdot}2SiO_2$) are the main mineral components. It is reasonable to approach the interpretation of high-calcia coal-ash with the help of the ternary system $CaO–Al_2O_3–SiO_2$.

After 807 operating hours of the gasifier, inspection and measurements indicated that serious spalling occurred to the refractory lining and two thirds of each brick have worn out in the upper portion of the straight side wall. A rapid change of temperature during too many emergency shutdowns, or other operational malfunctions of the plant, and poor thermal shock resistance of the original Brick-E material, on the one hand, should be considered as the major wear causes. On the other hand, microstructural alteration of the penetrated zone may cause more dangerous thermochemical spalling. This spalling repeats itself periodically following the sequence of crack formation and slag penetrations, followed by a stress build-up on the boundary between the penetrated zone and the bulk of the brick due to differences in thermal coefficients of expansion as a result of chemical, i.e. mineralogical, changes. The stress build-up could be followed by spalling of a brick layer (10–30 mm is common). About 50 mm diameter lumps of the brick were found in the gasifier. After the breakdown, the sequence starts again from the beginning. The thermochemical spalling effect could be reduced by controlling the slag penetration into the refractory body.

**Table 3. Mineral composition of slag in gasifier (%)**

| Slag | Metal | $CAS_2$ | $C_2AS$ | Spinel | Pyroxene | Glass |
|---|---|---|---|---|---|---|
| 1 | — | 40–50 | 5 | 15–20 | 15 | 20 |
| 2 | — | — | 60 | 30 | 10 | — |
| 3 | — | 50–55 | 40 | 5–10 | — | — |
| 4 | — | 55 | — | 10 | 15–20 | 15 |
| 5 | <1 | 55 | 15 | — | — | 30 |

Slags 1 and 2 are coated on the brick surface. Slags 3, 4 and 5 are present in the brick crack.

## 4 CONCLUSION

The following conclusions can be drawn from the work presented in this paper:

- Limestone was a good fluxing agent for Qiwu coal. The AFTs and viscosity of Qiwu coal slag basically decreased with an increase of CaO added. When the CaO/ash ratio was greater than 25% in the mixture of Qiwu coal and limestone, AFTs no longer reduced. The slag viscosity for limestone addition with CaO/ash = 25% was very low and in a narrow range (4–13 Pa·s) at temperatures between 1300°C and 1500°C. This meets the requirement that a coal gasifier could operate at lower temperature and tap slag smoothly.
- The corrosion resistance of the $ZrO_2$-bearing chromia refractories reduced with increasing CaO content in the coal slag. Increased chromia content in these refractory systems resulted in increased corrosion resistance.
- Coal slag penetration more easily deteriorated the microstructure of lower-chromia materials. The $ZrO_2$-bearing 90% $Cr_2O_3$ refractory with the lowest $SiO_2$ content could best retain its original microstructure. Thermochemical spalling of the $ZrO_2$-bearing 80% $Cr_2O_3$ refractory was considered as the primary attack mechanism during the trial operating period of the coal gasifier.

## REFERENCES

1. LIM, K. H., Investigations and design considerations for the refractory lining of coal gasifiers. *Int. Ceram.*, **32**(4) (1983) 34–37.
2. GUO, Z. Q., Progress in refractories for slagging coal gasifiers. *Industrial Ceramics*, **14**(1) (1994) 7–12.
3. HUGGINS, F. E., KOSMACK, D. A. & HUGGMAN, G. P., Correlation between ash-fusion temperatures and ternary equilibrium phase diagrams. *Fuel*, **60**(7) (1981) 577–584.